Evaluation of dynamical spectra for zero-temperature quantum Monte Carlo simulations: Hubbard lattices and continuous systems

J. J. Deisz

Department of Physics, Georgetown University
Washington, DC 20057, USA

W. von der Linden

Max-Planck-Institut für Plasmaphysik, EURATOM Association
D-85740 Garching b. München, Germany

R. Preuss and W. Hanke

Institut für Theoretische Physik, Universität Würzburg, Am Hubland
D-97074 Würzburg, Germany

Abstract. Dynamical spectra for Hubbard lattices and simple atoms are obtained using ground state projection (zero-temperature) quantum Monte Carlo and the maximum entropy method. For Hubbard lattices we show that results are equivalent to those obtained from maximum entropy deconvolutions of low-temperature grand canonical quantum Monte Carlo data. These calculations are resolution limited and fail to produce the discrete structure of the bound excited states of hydrogen, although integrated moments of the spectrum are accurate. However, low-energy structures from *ab initio* calculations can be incorporated into the maximum entropy default model to improve the accuracy of this method.

1. Quantum Monte Carlo, the maximum entropy method, and dynamical spectral

Quantum Monte Carlo (QMC) algorithms have been developed for a variety of systems and models, including the electron gas model, atoms and molecules, the Heisenberg spin model, Anderson impurity models, and Hubbard lattice models. To within statistical precision QMC calculations directly provide equal-time and static ($\omega = 0$) quantities, such as energy, compressibility, equal-time correlations, and static susceptibilities. Dynamical quantities ($\omega \neq 0$) are not calculated directly in QMC, but it has always been considered desirable to obtain spectral features in order to interpret electrical resistivity measurements, neutron scattering, photoemission, and other dynamical probes. Substantial progress has been made in developing an algorithm for obtaining dynamical

properties from finite-temperature quantum simulations. In this paper we demonstrate that this algorithm is applicable to zero-temperature QMC simulations, which we illustrate with a one-dimensional Hubbard lattice model and hydgrogen and helium atoms.

A typical quantity evaluated in finite-temperature simulations is the single-particle Green's function,

$$G(\mathbf{k},\tau) = - < \mathcal{T}_\tau e^{(\hat{H}-\mu\hat{N})\tau}\, \hat{c}_{\mathbf{k},\sigma}\, e^{-(\hat{H}-\mu\hat{N})\tau} \hat{c}^\dagger_{\mathbf{k},\sigma} >, \tag{1}$$

where the brackets indicate the canonical or grand-canonical ensemble average. Since finite temperature QMC simulations are based upon imaginary-time Feynman path-integrals [1], imaginary-time correlations like Eq.(1) are obtained directly. $G(\mathbf{k},\tau)$ is related to the single-particle spectral function, $A(\mathbf{k},\varepsilon)$,

$$\begin{aligned} A(\mathbf{k},\varepsilon) \quad &= \quad \frac{1}{\mathcal{Z}} \sum_{s,s'} e^{-\beta(E_s-\mu N_s)}(1+e^{-\beta\varepsilon}) \mid < s|\hat{c}_{\mathbf{k},\sigma}|s' > \mid^2 \\ &\quad \times\delta(\varepsilon - (E_{s'} - E_s - \mu)), \end{aligned} \tag{2}$$

by the integral transformation

$$G(\mathbf{k},\tau) = -\int_{-\infty}^{\infty} \frac{e^{-\varepsilon\tau}}{1+e^{-\varepsilon\beta}}\, A(\mathbf{k},\varepsilon)\, d\varepsilon. \tag{3}$$

However, deconvolution of Eq.(3) to obtain $A(\mathbf{k},\varepsilon)$ from QMC results for $G(\mathbf{k},\tau)$ is an ill-posed problem as the QMC data set for $G(\mathbf{k},\tau)$ is both noisy and finite.

The maximum entropy method (MEM) has been successfully applied to obtain approximate results from Eq.(3). MEM produces a unique result for $A(\mathbf{k},\varepsilon)$ by biasing towards a default model, $m(\varepsilon)$, which is chosen on the basis of perturbation theory [4], sum-rules [5, 6], or simply taken as constant. Biasing is affected by maintaining large values for the entropy functional,

$$S(A,m) = -\int_{-\infty}^{\infty} d\varepsilon\, [A(\mathbf{k},\varepsilon)\ln(A(\mathbf{k},\varepsilon)/m(\varepsilon)) - A(\mathbf{k},\varepsilon) + m(\varepsilon)]. \tag{4}$$

There are several choices for balancing between default model bias and producing a tight fit to QMC results for $G(\mathbf{k},\tau)$ [3]. It is generally true that the MEM result for $A(\mathbf{k},\varepsilon)$ has the favorable property that spectral features appear relative to $m(\varepsilon)$ only if justified by QMC data. Thus, spurious results from the ill-posed deconvolution are avoided.

The success of this scheme is evident in the number of systems to which it has been successfully applied, such as Anderson impurity models [4], one- and two-dimensional Hubbard lattices [7, 6], and Heisenberg antiferromagnets

[8, 9]. MEM deconvolutions are now a standard tool for analysis of data from finite-temperature QMC simulations.

This is not yet the case for zero-temperature or ground state calculations, possibly due to the lack of a periodic time-axis to make time-dependent functions simple to identify. Nonetheless, it has been shown that such time-dependent correlations can be evaluated for both Hubbard lattice systems [10] and two-electron atoms and molecules [11].

Imaginary-time ground-state expectation values are given by,

$$S_{\hat{Q}\hat{Q}}(\tau) \equiv < \hat{Q}^\dagger(\tau)\,\hat{Q}\,(\tau=0) > \equiv < \psi_o | e^{\tau \hat{H}}\,\hat{Q}^\dagger\,e^{-\tau \hat{H}}\,\hat{Q} | \psi_o >, \tag{5}$$

where $|\psi_o>$ is the ground state. $S_{\hat{Q}\hat{Q}}(\tau)$ has the spectral decomposition

$$S_{\hat{Q}\hat{Q}}(\tau) = \sum_m e^{-(E_m - E_o)\,\tau}\,|\,<\psi_m|\hat{Q}|\psi_o>|^2 \tag{6}$$

which is related to the dynamical structure factor or spectral function,

$$S_{\hat{Q}\hat{Q}}(\omega) = \sum_m |\,<\psi_m|\hat{Q}|\psi_o>|^2 \delta(\omega - (E_m - E_o)) \tag{7}$$

by a Laplace transform,

$$S_{\hat{Q}\hat{Q}}(\tau) = \int_0^\infty e^{-\omega\tau}\,S_{\hat{Q}\hat{Q}}(\omega)\,d\omega. \tag{8}$$

Thus, once imaginary-time correlation functions are evaluated, the extraction of dynamical information via Eq.(8) is essentially equivalent to obtaining dynamical information at finite temperature. We will demonstrate that the zero-temperature dynamical method suggested for Hubbard lattices [10] is as effective as the finite-temperature calculations which have more numerously appeared in the literature. We also place dynamical calculations for continuous systems [11] in the QMC+MEM framework and demonstrate via calculation of dynamics for hydrogen and helium atoms the energy resolution one obtains in QMC studies of such systems.

2. Numerical evaluation of imaginary-time correlations for Hubbard lattice models

If a trial state, $|\psi_T>$, has a finite overlap with the ground state $|\psi_o>$;

$$<\psi_o|\psi_T> = c_o, \quad |c_o| > 0;$$

then, in the limit β is large, $\exp(-\beta\hat{H})$ projects the ground state from $|\psi_T>$:

$$e^{-\beta\hat{H}}|\psi_T> \;=\; \sum_m e^{-\beta E_m} <\psi_m|\psi_T>\,|\psi_m> \tag{9}$$

$$\simeq\; e^{-\beta E_o} <\psi_o|\psi_T>\,|\psi_o>, \quad \beta\to\infty. \tag{10}$$

Defining $\tilde{S}_{\hat{Q}\hat{Q}}(\tau|\beta_1,\beta_2,\psi_T)$ as

$$\tilde{S}_{\hat{Q}\hat{Q}}(\tau|\beta_1,\beta_2,\psi_T) = \frac{<\psi_T|e^{-\beta_2\hat{H}}\, e^{\tau\hat{H}}\, \hat{Q}^\dagger\, e^{-\tau\hat{H}}\, \hat{Q}\, e^{-\beta_1\hat{H}}|\psi_T>}{<\psi_T|e^{-\beta_2\hat{H}}\, e^{-\beta_1\hat{H}}|\psi_T>} \tag{11}$$

and choosing β_1 and β_2 sufficiently large so that

$$e^{-\beta_1\hat{H}}|\psi_T> \simeq c_o\, e^{-\beta_1 E_o}|\psi_o> \tag{12}$$

and

$$e^{-(\beta_2-\tau)\hat{H}}|\psi_T> \simeq c_o\, e^{-(\beta_2-\tau)E_o}|\psi_o>, \tag{13}$$

then

$$\tilde{S}_{\hat{Q}\hat{Q}}(\tau|\beta_1,\beta_2,\psi_T) \simeq S_{\hat{Q}\hat{Q}}(\tau). \tag{14}$$

Henceforth, it is assumed that β_1, β_2 are sufficiently large so that the difference between $\tilde{S}_{\hat{Q}\hat{Q}}$ and $S_{\hat{Q}\hat{Q}}$ is exponentially small and can be ignored.

When $\hat{H}$ is the Hamiltonian for interacting particles, analytic results for Eq.(11) are generally unobtainable and numerical solution rapidly becomes infeasible as the size of the multi-particle Hilbert space increases. However, a Monte Carlo algorithm for evaluating Eq. (11) for equal time operators ($\tau = 0$) has been developed and implemented for Hubbard lattice models [**?**] described by Hamiltonia of form

$$\hat{H} = \hat{H}_o + \hat{H}_I \tag{15}$$

where

$$\hat{H}_o = \sum_{\mathbf{k},\sigma} \epsilon_{\mathbf{k}} \hat{n}_{\mathbf{k},\sigma} \tag{16}$$

is the hopping or kinetic energy part of the Hamiltonian and

$$\hat{H}_I = U \sum_{\mathbf{r},\sigma} \hat{n}_{\mathbf{r},\uparrow}\hat{n}_{\mathbf{r},\downarrow} \tag{17}$$

describes on-site Coulomb repulsion. We briefly review here the algorithm with the finite τ extension.

Without approximation $S_{\hat{Q}\hat{Q}}(\tau)$ is written as

$$\begin{aligned} S_{\hat{Q}\hat{Q}}(\tau) \;=\; & <\psi_T|(\prod_{i_L=m}^{1} e^{-\Delta\tau\hat{H}})\,\hat{Q}^\dagger\,(\prod_{i_R=m+m'-l+1}^{m+m'} e^{-\Delta\tau\hat{H}}) \\ & \times\hat{Q}\,(\prod_{i_R=1}^{m+m'-l} e^{-\Delta\tau\hat{H}})|\psi_T> \\ & \div <\psi_T|\prod_{i_L=m}^{1} e^{-\Delta\tau\hat{H}} \prod_{i_R=1}^{m+m'} e^{-\Delta\tau\hat{H}}|\psi_T>, \end{aligned} \tag{18}$$

where m is the number of the intervals of size $\Delta\tau$ used to project the ground state from the trial function,

$$m\,\Delta\tau = \beta_1 = \beta_2 - \tau_{max}, \tag{19}$$

and $m'+1$ is the number of imaginary-time values between $\tau = 0$ and τ_{max} where correlation functions are evaluated,

$$l\,\Delta\tau = \tau, \quad l = 0, 1, \cdots, m'. \tag{20}$$

$2m + m'$ exponential operators, $\exp(-\Delta\tau\,\hat{H})$, appear in Eq. (11), only the relative position of $\hat{Q}$ changes within the operator products. This permits evaluation of correlation functions for all τ values with a single simulation. $\Delta\tau$ is taken to be sufficiently small so that the Trotter approximation,

$$e^{-\Delta\tau(\hat{H}_o+\hat{H}_I)} = e^{-\Delta\tau\hat{H}_o/2}e^{-\Delta\tau\hat{H}_I}e^{-\Delta\tau\hat{H}_o/2} + \mathcal{O}(\Delta\tau^3), \tag{21}$$

remains accurate when terms of order $\Delta\tau^3$ are ignored. The discrete Hubbard-Stratonovic transformation [15];

$$e^{-\Delta\tau n_{i,\uparrow}n_{i,\downarrow}} = \frac{1}{2}\sum_{\sigma=\pm1} e^{2a\sigma(n_{i,\uparrow}-n_{i,\downarrow})-U\Delta\tau(n_{i,\uparrow}+n_{i,\downarrow})/2}, \tag{22}$$

$$\tanh^2 a = \tanh(\Delta\tau\,U/4); \tag{23}$$

transforms Eq.(18 to

$$S_{\hat{Q}\hat{Q}}(\tau) = \frac{\sum_{\sigma_{i,\mathbf{r}}} W(\sigma)\, S^{\sigma}_{\hat{Q}\hat{Q}}(\tau)}{\sum_{\sigma_{i,\mathbf{r}}} W(\sigma)} \tag{24}$$

where

$$S^{\sigma}_{\hat{Q}\hat{Q}}(\tau) = < \psi_T|(\prod_{i_L=m}^{1} e^{-\Delta\tau\hat{h}(\sigma_{i_L})}\,\hat{Q}^{\dagger}\,(\prod_{i_R=m+m'-l+1}^{m+m'} e^{-\Delta\tau\hat{h}(\sigma_{i_L})})$$

$$\times\hat{Q}\,(\prod_{i_R=1}^{m+m'-l} e^{-\Delta\tau\hat{h}_{\sigma_{i_R}}})|\psi_T>$$

$$\div < \psi_T|\prod_{i_L=m}^{1} e^{-\Delta\tau\hat{h}(\sigma_{i_L})} \prod_{i_R=m+}^{1}$$

and

$$W(\sigma) = < \psi_T|\prod_{i_L=1}^{m+m'} e^{-\Delta\tau\hat{h}(\sigma_{i_L})} \prod_{i_R=m}^{1} e^{-\Delta\tau\hat{h}(\sigma_{i_R})}|\psi_T> . \tag{26}$$

Each configuration of fields, $\sigma_{i,\mathbf{r}}$, (space and/or time indices for σ are not always explicitly given in the above and subsequent expressions) describes a

spatially- and time-dependent non-interacting fermion system. The advantage of evaluating $W(\sigma)$ and $S^{\sigma}_{\hat{Q}\hat{Q}}(\tau)$ for a non-interacting system is gained at the expense of having to evaluate these expressions for all field configurations $\sigma_{i,\mathbf{r}}$. This is generally prohibitive since a large number of fields is needed to make the Trotter approximation accurate. However, when $W(\sigma)$ is positive definite, or nearly so, importance sampling techniques are used to obtain $S_{\hat{Q}\hat{Q}}(\tau)$ to within statistical precision.

Evaluation of $W(\sigma)$ and $S^{\sigma}_{\hat{Q}\hat{Q}}(\tau)$ begins by choosing a trial state which on the basis of symmetry properties is expected to have a finite overlap with the ground state. $|\psi_T>$ is taken to be a single Slater determinant,

$$|\psi_T>=\hat{c}^{\dagger}_N \ \cdots \ \hat{c}^{\dagger}_1|0> \tag{27}$$

where, $\hat{c}^{\dagger}_1$ is the creation operator for a particle in the state with quantum numbers described by the number "1." Because the Hubbard-Stratonivich transformation produces Hamiltonia, $\hat{h}(\sigma_{i,\mathbf{r}})$, without particle-particle interactions, the evolved state remains a Slater determinant,

$$\prod_{i=1}^{N_{steps}} e^{-\Delta\tau\,\hat{h}(\sigma_i)}\hat{c}^{\dagger}_N \ \cdots \ \hat{c}^{\dagger}_1|0>=\hat{\tilde{c}}^{\dagger}_{N,1\rightarrow N_{steps}} \ \cdots \ \hat{\tilde{c}}^{\dagger}_{N,1\rightarrow N_{steps}}|0>, \tag{28}$$

where

$$\hat{\tilde{c}}^{\dagger}_{n,1\rightarrow N_{steps}} = \prod_{i=1}^{N_{steps}} e^{-\Delta\tau\,\hat{h}(\sigma_i)}\ \hat{c}^{\dagger}_n \prod_{i=N_{steps}}^{1} e^{\Delta\tau\,\hat{h}(\sigma_i)} \tag{29}$$

$$= \sum_{\mathbf{r}} < \phi_{\mathbf{r}}|\tilde{\phi}_{n,1\rightarrow N_{steps}} > \hat{c}^{\dagger}_{\mathbf{r}}. \tag{30}$$

The norm of the imaginary-time propagated single-particle state described by the operator $\hat{\tilde{c}}^{\dagger}_{n,1\rightarrow N_{steps}}$ does not remain equal to unity. Further, unlike the real-time propagator, the overlap of single-particle states does not remain constant. For fermion systems only the orthogonal components of the $\hat{\tilde{c}}^{\dagger}_{n,1\rightarrow N_{steps}}$. It is perfectly valid and necessary for numerical stability to periodically orthogonalize the N-single electron states as they are evolved in imaginary time.

After these state are evolved through all time steps the weight function becomes,

$$W(\sigma)=<0|\hat{\tilde{c}}_{1,1_L\rightarrow m_L} \cdots \hat{\tilde{c}}_{N,1_L\rightarrow m_L}\ \hat{\tilde{c}}^{\dagger}_{N,1_R\rightarrow m+m'_R} \cdots \hat{\tilde{c}}^{\dagger}_{1,1_R\rightarrow m+m'_R}|0>, \tag{31}$$

whose numerical value is given by the determinant of the single-particle overlap matrix,

$$W(\sigma)=\mathrm{Det}\ <\tilde{\psi}_{i,1_L\rightarrow m_L}|\tilde{\psi}_{j,1_R\rightarrow m+m'_R}>. \tag{32}$$

For the evaluation of $S^{\sigma}_{\hat{Q}\hat{Q}}(\tau)$ we consider the operators $\hat{Q} = \hat{c}^{\dagger}_{\mathbf{r}}$, $\hat{Q}^{\dagger} = \hat{c}_{\mathbf{r}'}$

$$S_{\hat{Q}\hat{Q}} \equiv G^{+}(\mathbf{r},\tau;\mathbf{r}',\tau=0) \equiv < \psi_o | e^{\hat{H}\tau}\, \hat{c}_{\mathbf{r}}\, e^{-\hat{H}\tau}\, \hat{c}^{\dagger}_{\mathbf{r}'} | \psi_o > \tag{33}$$

describes the particle-addition spectrum. To evaluate the numerator of Eq.(11), the trial function is first propagated $m + m' - l$ steps,

$$\prod_{i_R=1}^{m+m'-l} e^{-\Delta\tau\, \hat{h}(\sigma_{i_R})} |\psi_T > = \hat{\hat{c}}^{\dagger}_{N,(1_R \rightarrow m+m'-l_R)} \cdots \hat{\hat{c}}^{\dagger}_{N,(1_R \rightarrow m+m'-l_R)} |0>, \tag{34}$$

upon which a particle is added at $\mathbf{r}'$,

$$\hat{c}^{\dagger}_{\mathbf{r}'} \prod_{1}^{i_R=m+m'-l} e^{-\Delta\tau\, \hat{h}(\sigma_{i_R})} |\psi_T > = \hat{c}^{\dagger}_{\mathbf{r}'}\, \hat{\hat{c}}^{\dagger}_{N,(1_R \rightarrow m+m'-l_R)} \cdots \hat{\hat{c}}^{\dagger}_{1,(1_R \rightarrow m+m'-l_R)} |0> \tag{35}$$

and that state is propagated l more time steps,

$$\prod_{i_R=m+m'-l}^{m+m'} e^{-\Delta\tau\, \hat{h}(\sigma_{i_R})} \hat{c}_{\mathbf{r}'} \prod_{i_R=1}^{m} e^{-\Delta\tau\, \hat{h}(\sigma_{i_R})} = \hat{\hat{c}}_{\mathbf{r}',m+m'-l_R \rightarrow m+m'_R} \hat{\hat{c}}^{\dagger}_{N,1_R \rightarrow m+m'_R} \cdots \hat{\hat{c}}^{\dagger}_{1,1_R \rightarrow m+m'_R} |0> \tag{36}$$

yielding

$$\begin{aligned} G^{+\sigma}(\mathbf{r},\tau;\mathbf{r}',\tau=0) \;\; = \;\; & < 0 | \hat{\hat{c}}_{1,1_L \rightarrow m_L} \;\cdots\; \hat{\hat{c}}_{N,1_L \rightarrow m_L}\, \hat{c}_{\mathbf{r}}\, \hat{\hat{c}}_{\mathbf{r}'} \\ & \times m + m' - l_R \rightarrow m + m'_R\, \hat{\hat{c}}^{\dagger}_{N,1 \rightarrow m+m'_R} \;\cdots\; \hat{\hat{c}}^{\dagger}_{1,1_R \rightarrow m+m'_R} |0> \\ & \div < 0 | \hat{\hat{c}}_{1,1_L \rightarrow m_L} \;\cdots\; \hat{\hat{c}}_{N,1_L \rightarrow m_L}\, \hat{\hat{c}}^{\dagger}_{N,1_R \rightarrow m+m'_R} \;\cdots\; \hat{\hat{c}}^{\dagger}_{1,1_R \rightarrow m+m'_R} |0> . \end{aligned} \tag{37}$$

The numerator of this expression is, like the denominator, numerically equal to the determinant of the overlap matrix. N^2 of the elements of this $(N+1) \times (N+1)$ overlap are already calculated in evaluating $W(\sigma)$ and it is possible to evaluate this ratio without explicitly evaluating the determinant of the matrix represented by the numerator [**?**].

The above expression is nearly equivalent to the expression for evaluating equal-time Green's functions and it is possible to express $G^{+\sigma}(\mathbf{r},\tau;\mathbf{r}',\tau=0)$ in terms of equal-time Green's functions,

$$G^{+\sigma}(\mathbf{r},\tau;\mathbf{r}') = \sum_{r''} < \psi_{\mathbf{r}''} | \tilde{\psi}_{\mathbf{r}',m+m'-l_R,m+m'_R} > \; G^{+\sigma}(\mathbf{r},\tau=0;\mathbf{r}'',\tau=0), \tag{38}$$

i.e., the time-evolved particle addition Green's function is the sum of the $\tau = 0$ Green's functions weighted by the amplitude of for an the added electron to evolve from $\mathbf{r}'$ to position $\mathbf{r}''$. Evaluation of the amplitude $< \psi_{\mathbf{r}''} | \tilde{\psi}_{\mathbf{r}',m+m'-l_R,m+m'_R} >$ is a single-electron calculation with the Pauli exclusion principle accounted for in the determinants for the equal-time Green's function. Provided the calculation of the equal time Green's function has been stabilized, the naive use

of Eq.(38) leads to numerically stable results up to at least $\tau = 6$ for the calculations we are about to describe. It is possible, though, to periodically orthogonalize the orbital for the added particle with respect to the filled states in order to increase the stability of this operation.

Although thermal Green's functions obtained in finite temperature simulations describe both particle addition and subtraction, the particle-subtraction Green's function,

$$G^{-}(\mathbf{r},\tau;\mathbf{r}',\tau=0) \equiv < \psi_o | e^{\hat{H}\tau}\, \hat{c}^{\dagger}_{\mathbf{r}}\, e^{-\hat{H}\tau}\, \hat{c}_{\mathbf{r}'} | \psi_o > . \tag{39}$$

must be explicitly evaluated for zero temperature. The propagation of the annihilation operator is given by

$$\hat{\tilde{c}}_{\mathbf{r}',m+m'-l_R\rightarrow m+m'_R} = \prod_{i_R=m+m'-l}^{m+m'} e^{-\Delta\tau\hat{h}(\sigma_{i_R})} c_{\mathbf{r}'} \prod_{i_R=m+m'-l}^{m+m'} e^{\Delta\tau\hat{h}(\sigma_{i_R})} \tag{40}$$

$$= [\prod_{i_R=m+m'-l}^{m+m'} e^{\Delta\tau\hat{h}(\sigma_{i_R})} c^{\dagger}_{\mathbf{r}'} \prod_{i_R=m+m'-l}^{m+m'} e^{-\Delta\tau\hat{h}(\sigma_{i_R})}]^{\dagger} \tag{41}$$

The quantity in brackets describes the propagation of a particle starting at $\mathbf{r}'$ with Hamiltonia $\hat{h}' = -\hat{h}$. Thus,

$$G^{-\sigma}(\mathbf{r},\tau;\,\mathbf{r}',\tau=0) = \sum_{r''} < \tilde{\psi}'_{\mathbf{r}',(\mathbf{m+m'-l_R\rightarrow m+m'_R})} | \psi_{\mathbf{r}''} > G^{-\sigma}(\mathbf{r},\tau=0;\,\mathbf{r}'',\tau=0) \tag{42}$$

where the primed wave function, $\tilde{\phi}'$ indicates propagation with $-\hat{h}$.

Density, spin, and current correlation functions are evaluated in terms of $G^{+\sigma}$ and $G^{-\sigma}$ because of the applicability of Wick's theorem for a non-interacting systems. For example, the density correlation function

$$S_{nn}(\mathbf{r},\tau;\,\mathbf{r}';\tau=0) \equiv < \psi_o | e^{\hat{H}\tau}\, \hat{n}_{\mathbf{r}}\, e^{-\hat{H}\tau}\, \hat{n}_{\mathbf{r}'}\, | \psi_o > \tag{43}$$

is determined from

$$S^{\sigma}_{nn}(\mathbf{r},\mathbf{r}';\tau) = G^{+\sigma}(\mathbf{r},\tau;\mathbf{r},\tau)G^{+\sigma}(\mathbf{r}',\tau=0;\mathbf{r}',\tau=0) + G^{+\sigma}(\mathbf{r},\tau;\mathbf{r}',\tau=0)G^{-\sigma}(\mathbf{r},\tau;\mathbf{r}',\tau=0) \tag{44}$$

where a third single-electron Green's function is evaluated,

$$G^{+\sigma}(\mathbf{r},\tau;\mathbf{r},\tau) = \sum_{\mathbf{r}',\mathbf{r}''} < \tilde{\psi}'_{\mathbf{r},m+m'-l_R\rightarrow m+m'} | \psi_{\mathbf{r}'} > \tag{45}$$

$$\times < \psi_{\mathbf{r}''} | \tilde{\psi}_{\mathbf{r},m+m'-l_R\rightarrow m+m'} G(\mathbf{r}',\tau=0;\,\mathbf{r}'',\tau=0),$$

which corresponds to a Green's function where both the annihilation and creation operator have been propagated to τ. While the average of this is the same as is that for $\tau = 0$, for a given field configuration they are different

and time-displacement is necessary for calculating multi-particle correlation functions.

Fig. 1 displays results for $G^+(r, \tau = 0)$ for the one-dimensional Hubbard model with $U = 4t$. For an equivalent sample size (20,000) these results are seen to be equivalent to those obtained with the grand canonical algorithm at low temperature ($T = t/16$). The lattice size, $L = 12$, is sufficiently small so that comparison may be made with results from exact diagonalization. We make this comparison on the real-frequency axis after continuing the τ-data using the maximum entropy method. As is typical for these calculations, the Monte Carlo and maximum entropy does not produce all of the discrete structure of the exact spectra, but provides a qualitatively correct description of the spectral distribution.

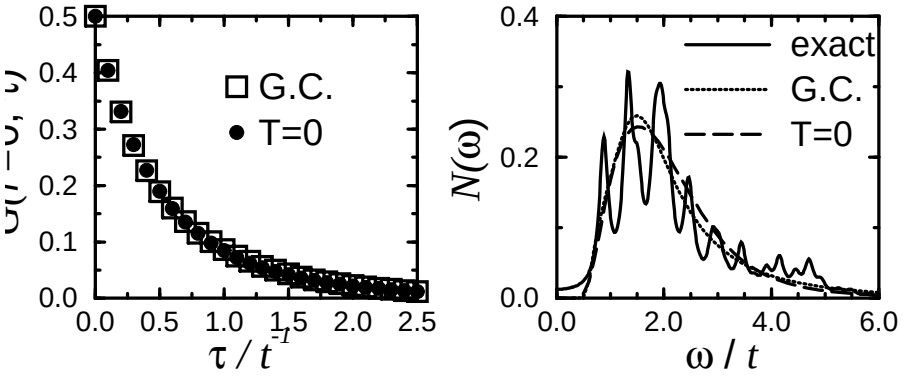

Figure 1: (a) Imaginary-time particle addition correlations from projector and grand-canonical quantum Monte Carlo for the half-filled Hubbard model with 12 sites and $U = 4t$. (b) Analytically continued particle-addition spectrum versus results from exact diagonalization. The grand canonical and projector Monte Carlo results are essentially equivalent, broadening the discrete structure of the exact result.

Since QMC + MEM dynamical results are correct only to within some resolution limit, quantities which are obtained by integrating over dynamical spectra are expected to reasonably accurate. For example, the Drude weight, the $\omega = 0$ of the optical conductivity is given by

$$D = - < H_o > -2 \int_0^\infty \frac{S_{jj}(\omega)}{\omega} d\omega \tag{46}$$

where $S_{jj}(\omega)$ is obtained by analytically continuing the current-current correlation function

$$S_{jj}(\tau) =< 0|e^{\hat{H}\tau}\hat{j}e^{-\hat{H},\tau}\hat{j}|0 > \tag{47}$$

where

$$\hat{j} = -it\sum_{\mathbf{r},\sigma}(\hat{a}^{\dagger}_{r,\sigma}\hat{a}_{r+1,\sigma} - \hat{a}^{\dagger}_{r+1,\sigma}\hat{a}_{r,\sigma}). \tag{48}$$

Fig.2 displays results for the Drude weight versus lattice size. For half-filling, D vanishes in the thermodynamic limit. The projector Monte Carlo results are in good agreement with respect to the finite-size dependence of this quantity.

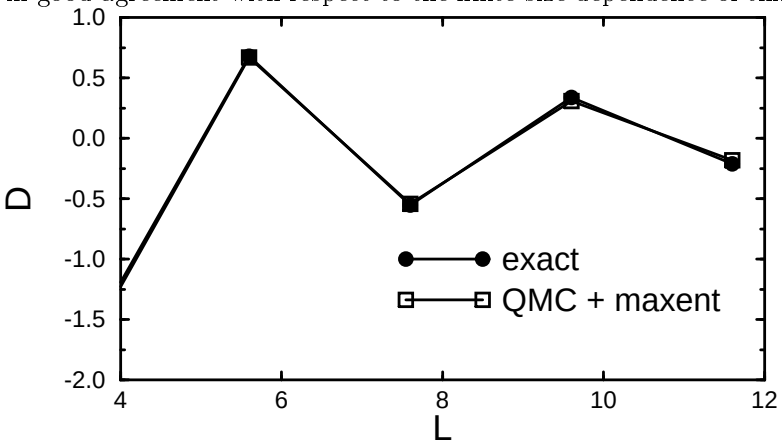

Figure 2: Finite-size dependence of the Drude weight as calculated from exact diagonalization and using a sum-rule with projector quantum Monte Carlo results for the one-dimensional half-filled Hubbard model with U=4.

3. Zero-temperature dynamical calculations for continuous systems.

The diffusion Monte Carlo algorithm (DMC) has been utilized for the electron gas model [16], atoms and molecules [17, 18], and periodic atomic lattices [19]. Like the Hubbard model algorithm, DMC uses $\exp(-\hat{H}t)$ as a ground-state projection operator. However, time-dependent particle configurations are sampled rather than Hubbard-Stratonovic fields. Nonetheless it is again possible to evaluate imaginary-time correlation functions of form Eq.(5).

The time-dependence of ground state projection,

$$|\Phi(t)>= e^{-t\hat{H}}\,|\Phi(t=0)>=\sum_m e^{-tE_m} < \Phi_m|\Phi(t=0)> \,|\Phi_m> . \quad (49)$$

is carried out in a coordinate representation $|\Phi(t)>$ is given by

$$|\Phi(t)>= \int d\mathbf{R}\phi(\mathbf{R},t)\,|\mathbf{R}>, \quad (50)$$

where the time-dependent amplitude is determined from the differential equation

$$-\frac{\partial\phi(\vec{R},t)}{\partial t} = [-D\nabla^2 + V(\vec{R})\,]\,\phi(\vec{R},t), \quad (51)$$

where $D \equiv \hbar^2/2m$, and $\mathbf{R}$ represents the $3N$ particle coordinates (the lowercase $\mathbf{r}$ indicated lattice positions for Hubbard calculations). Defining $f(\mathbf{R},t) \equiv f = \psi_T^*(\mathbf{R})\phi(\mathbf{R},t) =< \psi_T|\mathbf{R} >< \mathbf{R}|\Phi(t) >$ leads to a second differential equation,

$$-\frac{\partial f(\mathbf{R},t)}{\partial t} = -D\nabla^2 f(\mathbf{R},t) + E_{local}(\mathbf{R})\; f(\mathbf{R},t) + D\nabla\cdot[f(\mathbf{R},t)\vec{F}_Q(\mathbf{R})] \quad (52)$$

where $\vec{F}_Q(\mathbf{R}) \equiv \nabla(\ln|\psi_T(\mathbf{R})|^2)$ and $E_{loc}(\mathbf{R}) \equiv \hat{H}\psi_T(\mathbf{R})/\psi_T(\mathbf{R})$. The motivation for defining $f(\mathbf{R},t)$ is that $\phi(\mathbf{R},t)$ is generally both positive and negative while $f(\mathbf{R},t)$ will be nearly always positive if the nodal structure of $\psi_T(\mathbf{R})$ is reasonably close to that of the true ground state. This positivity makes $f(\mathbf{R},t)$ more suitable for developing a Monte Carlo algorithm.

Generally, Eq.(52) cannot be evaluated exactly. For small $\Delta\tau$,

$$\begin{aligned} G(\mathbf{R}'\rightarrow\mathbf{R}),\Delta\tau) &= (4\pi D\,\Delta\tau)^{-3N/2} && (53)\\ &\quad \exp(-\Delta\tau[E_{loc}(\mathbf{R}) + E_{loc}(\mathbf{R}')]/2) && (54)\\ &\quad \times\ \exp(-[\mathbf{R}' - \mathbf{R} - D\,\Delta\tau\vec{F}_Q(\mathbf{R})]^2/(4D\,\Delta\tau)\,) && (55)\end{aligned}$$

is a good approximation for the exact Green's function for Eq.(52) which satisfies

$$f(\mathbf{R},t+\tau) = \int d\mathbf{R}'\; G,\tau)\; f(\mathbf{R}',t). \quad (56)$$

The long-time limit is necessary for ground state projection so it is necessary to use repeated application of the approximation for the short-time Green's function:

$$\begin{aligned} f(\mathbf{R},n\Delta\tau) &= \int d\mathbf{R}_1\,\cdots\,d\mathbf{R}_n\,G(\mathbf{R}_n\rightarrow\mathbf{R},\Delta\tau)\,\cdots && (57)\\ &\quad G(\mathbf{R}_1\rightarrow\mathbf{R}_2,\Delta\tau)f(\mathbf{R}_1,t=0). && (58)\end{aligned}$$

The configurational average of E_{loc},

$$< E_{loc}(\mathbf{R}) >= \int d\mathbf{R}\, d\mathbf{R}_1\, \cdots\, W(\mathbf{R}, \mathbf{R}_n, \cdots \mathbf{R}_1) E_{loc}(\mathbf{R}) \tag{59}$$

where

$$W(\mathbf{R}, \mathbf{R}_n, \cdots \mathbf{R}_1) = \frac{f(\mathbf{R}_1, t=0) G(\mathbf{R}_1 \rightarrow \mathbf{R}_2, \Delta\tau) \cdots G(\mathbf{R}_n \rightarrow \mathbf{R}, \Delta\tau)}{\int d\mathbf{R} d\mathbf{R}_1 \cdots d\mathbf{R}_2 d\mathbf{R}_n\, f(\mathbf{R}_1, t=0)\; G(\mathbf{R}_1 \rightarrow \mathbf{R}_2, \tau)\; \cdots\; G(\mathbf{R}_n \rightarrow \mathbf{R}, \tau)}, \tag{60}$$

is equal to the ground-state energy in the long-time limit. For the hydrogen and helium atoms $W(\mathbf{R}, \mathbf{R}_1, \cdots \mathbf{R}_n)$ is positive definite and is used as the sampling weight for the particle configuration trajectory $(\mathbf{R}_1, ..., \mathbf{R}_n, \mathbf{R})$.

It is possible to evaluate averages of time-displaced operators that are functions of particle coordinates and spin,

$$\begin{aligned} & < \hat{Q}(t_1 = n_1\Delta\tau)\, \hat{Q}(t_1 + \tau = n_2\Delta\tau) > \qquad (61) \\ = & \int d\mathbf{R} d\mathbf{R}_1 d\mathbf{R}_n W(\mathbf{R}, \mathbf{R}_n, \cdots \mathbf{R}_{n_1}\; \cdots\; \mathbf{R}_{n_2}\, \mathbf{R}_1)\, Q(\mathbf{R}_{n_1})\, Q(\mathbf{R}_{n_2}). \end{aligned}$$

The significance of this average is determined via identities such as

$$\begin{aligned} & \int d\mathbf{R}' G(\mathbf{R}', \Delta\tau) Q(\mathbf{R}')\, f(\mathbf{R}', t) \qquad (62) \\ = & \sum_m e^{-E_m t} < \Phi_m | \Phi(t=0) > \int d\mathbf{R}' G(\mathbf{R}', \Delta\tau) \psi_T^*(\mathbf{R}') Q(\mathbf{R}') \phi_m(\mathbf{R}') \qquad (63) \\ = & \sum_{m,n} e^{-E_m t} < \Phi_m | \Phi(t=0) >< \Phi_n | \hat{Q} | \Phi_m > e^{-E_n \Delta\tau} \psi_T^*(\mathbf{R}) \phi_n(\mathbf{R}) \qquad (64) \end{aligned}$$

leads to the result

$$< \hat{Q}(t_1 = n_1\Delta\tau)\, \hat{Q}(t_1 + \tau = n_2\Delta\tau) >= \sum_m e^{-(E_m - E_o)\tau} | < \Phi_m | \hat{Q} | \Phi_o > |^2. \tag{65}$$

provided both $t - t_1 - \tau$ and t_1 are sufficiently large to project the ground-state via Eq.(9). This has the desired form of Eq.(6) so that MEM can be used to obtain dynamical spectra.

If Fig. 3(a) we show dipole correlation functions ($\hat{Q} = \sum_{i=1}^{N} \hat{x}_i$) for hydrogen and helium atoms. Using a flat default model for $0 \leq \omega \leq 6$a.u. leads to the MEM result represented by the solid line in Fig. 3(b). Like the Hubbard simulations, MEM fails to reproduce the discrete spectra. Integrated spectral features are obtained more accurately, such as the static polarizability, $\chi_{xx}(\omega = 0) = \int \omega^{-1} S_{xx}(\omega) d\omega = 2.246$ where the exact result is 2.25.

QMC-derived dynamical correlations for helium have been reported earlier for helium [11], but not within the MEM framework. The discrete bound-state spectrum beginning at $\Delta E_{^1S \rightarrow {}^3P} \simeq 0.78 a.u.$ is unresolved and merges with

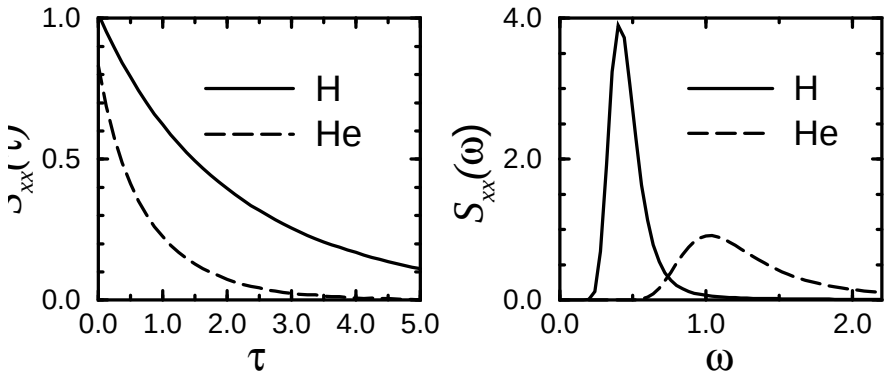

Figure 3: (a) Imaginary-time dipole correlations and (b) dipole excitation spectra for hydrogen and helium atoms in atomic units. Since excitations lie at high-frequency for these atoms, the quantum Monte Carlo + maximum entropy excitation spectra are very broad. Similar to the Hubbard lattice calculations, the qualitatively correct spectral distribution produces good results for frequency integrated quantities like the static polarizability. When the exact matrix element and frequency is included for the $1s \rightarrow 2p_x$ transiton of hydrogen (dotted line) structure related to the discrete spectrum begins to appear. This represents the compatability of *ab initio* and QMC calculations for obtaining the best possible spectrum.

excitations above the first ionization threshold at $\sim 0.9 a.u.$ The polarizability again agrees fairly well with the expected value, with QMC+MEM giving 0.657 which differs by 3% from the exact value ~ 0.675.

For systems with more than two electrons, this algorithm must be modified because of the "sign problem"; $G(\mathbf{R}' \rightarrow \mathbf{R}, \Delta\tau)$ is supplemented with a fixed-node constrint to ensure positivity [18], which leads to a variational upper bound for the ground state energy.

The restriction of paths to remain within a nodal surface of $\psi_T(\mathbf{R})$ prevents identification of Eq.(61) as the τ-dependent correlation function. However, when the true Green's function is used from time slice n_1 to n_2 and the fixed-node Green's function elsewhere, Eq.(61) becomes

$$< \hat{Q}(t_1 = n_1 \Delta\tau)\, \hat{Q}(t_1 + \tau = n_2 \Delta\tau) >_{FN} \tag{66}$$

$$= \sum_m |<\phi_o^{FN}|\hat{Q}|\phi_o^{FN}>|^2 e^{-E_m\tau} / \sum_m |<\phi_o^{FN}|\phi_m>|^2 e^{-E_m\tau} \quad (67)$$

W becomes negative in this calculation, but the average sign depends on τ rather than the longer time t needed for both ground state projection and dynamical propagation. We have not yet performed calculations to verify the usefulness of this approach.

Results from *ab initio* calculations can be used to improve these results. For atoms and molecules with a small number of electrons, accurate oscillator strengths and transition energies can obtained with *ab initio* methods. These results can be included in the default model, $m(\omega)$, so that MEM is not forced to reproduce the part of the spectrum which is known. This is especially valuable when the sign problem limits the τ values over which correlations can be evaluated. High-frequency parts of the spectrum are most strongly represented in the short-time correlations which may be accessible via Eq.(66).

In order to illustrate this idea, we have performed two MEM deconvolutions for hydrogen, both of which are shown in Fig. 3(b). The solid line is the spectrum derived using a flat default model which begins at zero-frequency. The dotted line used the exact oscillator strength and transition energy for the $1s \rightarrow 2p_x$ excitation. The dotted line begins to show the discrete structure of the hydrogen spectrum, but produces essentially equivalent results at high frequencies.

Acknowledgments

We would like to acknowledge useful conversations with F.F. Assaad. Part of this work was supported by a grant by the Deutsche Akadmischer Austauschdienst.

References

[1] J.W. Negele and H. Orland, *Quantum Many-Particle Systems*, (Addison-Wesley, Redwood City, 1988), ch. 8.

[2] R.N. Silver, D.S. Sivia, and J.E. Gubernatis, Phys. Rev. B **41**, 2380 (1990); and in *Quantum Simulations of Condensed Matter Phenomena*, edited by J.E. Gubernatis and J.D. Doll, (World Scientific, Singapore, 1990), p. 340.

[3] J.E. Gubernatis, M. Jarrell, R.N. Silver, and D.S. Sivia, Phys. Rev. B **44**, 6011 (1991).

[4] R.N. Silver, D.S. Sivia, J.E. Gubernatis, and M. Jarrell, Phys. Rev. Lett. **65**, 496 (1990).

[5] J. Deisz, M. Jarrell, and D.L. Cox, Phys. Rev. B **42**, 4869 (1990).

[6] S.R. White, Phys. Rev. B **44**, 4670 (1991).

[7] R. Preuss, A. Muramatsu, W. von der Linden, P. Dietrich, F.F. Assaad, and W. Hanke, Phys. Rev. Lett **73**, 732 (1994).

[8] J. Deisz, M. Jarrell, and D.L. Cox, Phys. Rev. B **48**, 10227 (1993).

[9] M. Macivić and M. Jarrell, Phys. Rev. Lett **68**, 1770 (1992).

[10] W. von der Linden, Phys. Rep. **220**, 53 (1992).

[11] M. Caffarel, M. Réraf, and C. Pouchan, Phys. Rev. A **47**, 3704 (1993).

[12] S. Sorella, E. Tosatti, S. Baroni, R. Car, and M. Parinello, *Proc. Adriatico Research Conf. Towards the Theoretical Understanding of the High-T_c Superconductors*, eds. S. Lundqvist, E. Tosatti, M. Tosi, and L. Yu (World Scientific, Singapore, 1988).

[13] S. Sorella, S. Baroni, R. Car, and M. Parinello, Europhys. Lett. **8**, 663 (1989).

[14] W. von der Linden, I. Morgenstern, and H. De Raedt, Phys. Rev. B **41**, 4669 (1990).

[15] J.E. Hirsch, Phys. Rev. B **28**, 4059 (1983); Phys. Rev. Lett. **51**, 1900 (1983); Phys. Rev. B **31**, 4403 (1985).

[16] D.M. Ceperly and B.J. Alder, Phys. Rev. Lett. **45**, 566 (1980).

[17] B.J. Alder, D.M. Ceperly, and P.J. Reynolds, J. Phys. Chem. **86**, 1200 (1982).

[18] P.J. Reynolds, D.M. Ceperly, B.J. Alder, and W.A. Lester, Jr., J. Chem. Phys. **77**, 5593 (1982).

[19] X.-P. Li, D.M. Ceperly, and R.M. Martin, Phys. Rev. B **44**, 10929 (1991).